

## Supporting Information

Trapping and visualizing intermediate steps in the mismatch repair pathway *in vivo*

**Justin S. Lenhart<sup>1§</sup>, Monica C. Pillon<sup>2§</sup>, Alba Guarné<sup>2</sup> and Lyle A. Simmons<sup>1\*</sup>**

The supplemental information contains “Experimental Procedures”, 7 figures, and 2 tables.

### Experimental Procedures

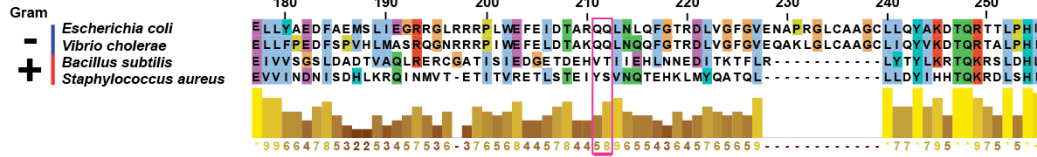
#### Quantitative Western blotting (LiCOR) analysis.

Whole cell lysates were prepared from independent JSL364 (wild-type) and JSL281 (*AmutS*) strains in 6 mL cultures (S7<sub>50</sub> minimal media supplemented with 2% D-Glucose) grown at 30°C and harvested at a normalized OD<sub>600</sub> of 0.5, while simultaneously plated for viables (10<sup>-6</sup> dilution, see *Spontaneous mutation rate analysis* in the main text). Cells were pelleted and incubated in 1 mL of lysis buffer (10 mM Tris HCl [pH 7.5], 1 mM EDTA, 10 mM MgCl<sub>2</sub>, 1 mM AEBSF, 0.5 mg/mL lysozyme, and 0.1mg/mL DNase I) and incubated at 37°C for 10 minutes. After incubation, SDS was added to a final concentration of 1% to lyse cells. Cells were heated for 5 minutes at 100°C and lysates concentrated to a known final volume in a 10 kDa concentrator column (Amicon Ultra Centrifugal Filters, Millipore).

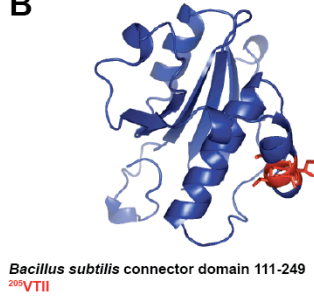
Immunodot blotting was performed essentially as described (Klocko *et al.*, 2011) and as described in “Material and Methods” in the main text. Briefly, whole cell lysates were immobilized onto a nitrocellulose membrane via wet transfer using the mini Trans-Blot electrophoresis transfer cell in transfer buffer without SDS (Bio Rad). The membrane was incubated in blocking buffer (5% milk solids, 17.4 mM Na<sub>2</sub>HPO<sub>4</sub>, 2.6 mM NaH<sub>2</sub>PO<sub>4</sub>, 150 mM

NaCl) at 22°C for one hour. All subsequent washes and incubations took place in blocking buffer. After blocking, the membrane was incubated with primary antisera  $\alpha$ -MutS (MI 1042) in blocking buffer (minus tween-20) overnight at 4°C with constant agitation. The next morning, the blot was washed three times for 15 minutes each in blocking buffer supplemented with 0.05% Tween-20. After washing, the blots were then incubated in the dark in 1:15,000 Odyssey Goat anti-Rabbit IR Dye 800CW (926-32211, LiCOR Biosciences) at 22°C for 2 hours in blocking buffer. All subsequent steps were performed in the dark. The blot was then washed 3 more times in blocking buffer with 0.05% Tween-20, followed by a wash in PBST (17.4 mM Na<sub>2</sub>HPO<sub>4</sub>, 2.6 mM NaH<sub>2</sub>PO<sub>4</sub>, 150 mM NaCl, 0.05% Tween-20) to remove excess milk solids. Membranes were dried for 2 hours followed by exposure using an Odyssey CLx Infrared Imaging System (LiCOR, Lincoln, Nebraska). All data analysis and band quantifications were performed using the Odyssey CLx software.

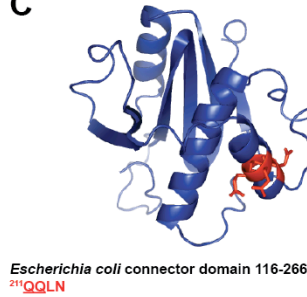
A



B



C



D

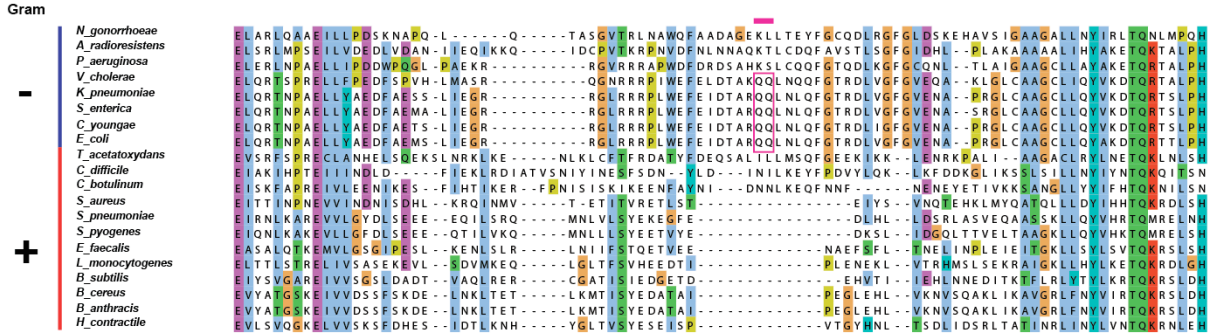


**Figure S1. The *E. coli* MutS di-glutamine (Q211 and Q212) binding site for MutL is not conserved in *B. subtilis* MutS.** A) A sequence alignment directly comparing the MutS amino acid sequence of the Gram-negative bacteria *E. coli* and *V. cholerae* to the MutS amino acid sequence of the Gram-positive bacteria *B. subtilis* and *S. aureus*. The region surrounding the di-glutamine MutL docking site (underlined in pink) is shown. The alignment was generated using the <http://www.ebi.ac.uk/Tools/msa/clustalw2/> server. The residue numerical designations shown above the alignment are relative to the *E. coli* amino acid sequence. Protein structure models of the B) *B. subtilis* (Phyre2 server model) and the C) *E. coli* connector domain (PDB file 1E3M). Shown in red are the residues corresponding to either the <sup>205</sup>VTII site in *B. subtilis* or the <sup>211</sup>QQLN of *E. coli*. D) A sequence alignment generated employing the

<http://www.ebi.ac.uk/Tools/msa/clustalo/> server to visualize the conservation of the QQ site in *E. coli* shown in both Gram-positive and negative bacteria. The order within the alignment is based on a phylogenetic organization of aligned MutS homologs using a Neighbour-joining tree without distance corrections.

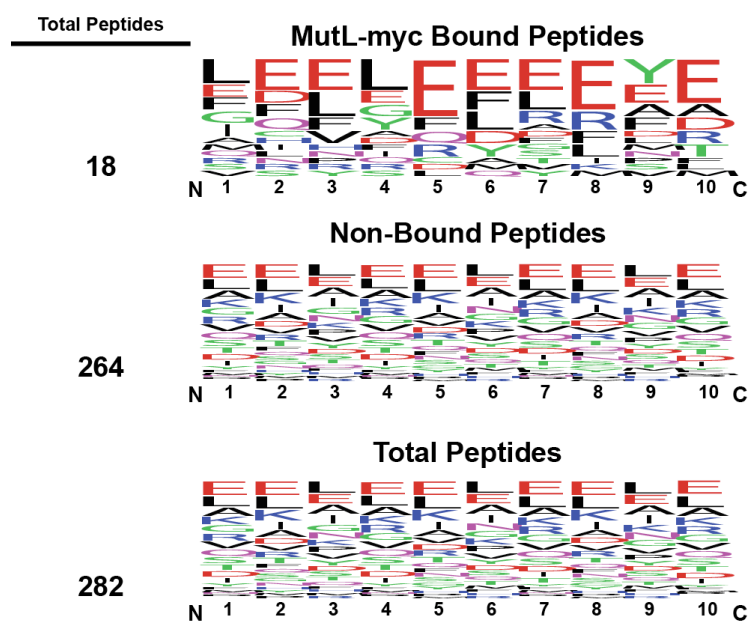


**Figure S2. Amino acid composition of MutS peptides recognized by MutL.** Analysis of the amino acid composition of MutL interaction peptides, MutL non-bound peptides, and total MutS peptides in the peptide array. Results visualized with WebLogo 3.1.

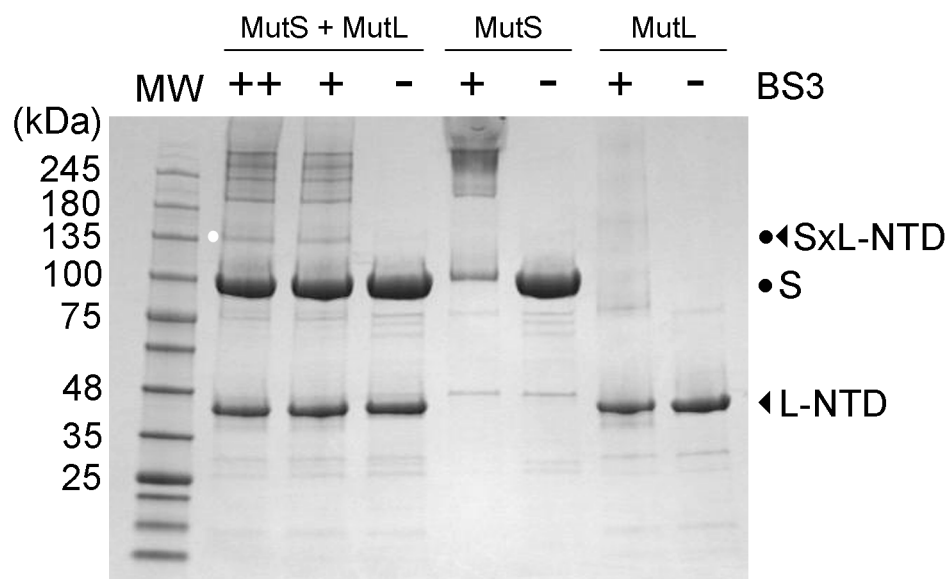


**Figure S3. Crosslinking of wild type MutS to the N-terminal domain of MutL with homoduplex DNA.** Mixtures of each protein, 10 mM ATP, and a 90 base-pair homoduplex DNA were incubated with the chemical crosslinker BS3 (+=0.8 mM and +=1.6 mM, respectively). Protein complexes were then separated on a 4-15% gradient SDS polyacrylamide gel. The bands corresponding to the MutS and MutL-NTD monomers, as well as the MutS•MutL-NTD complex are labeled.

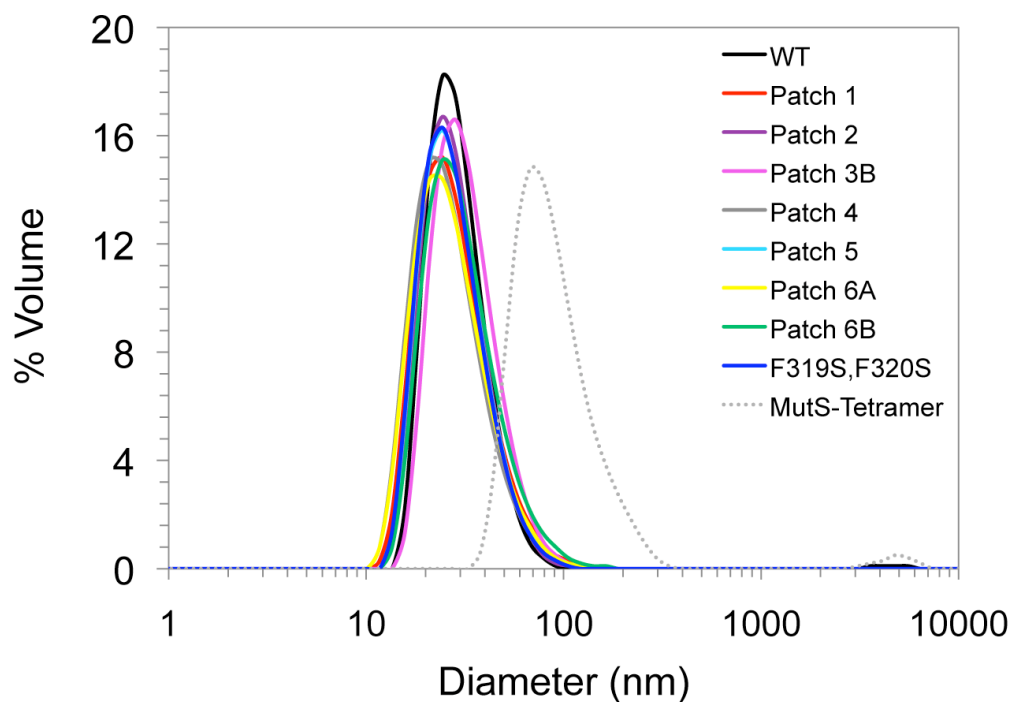


**Figure S4. Characterization of the particle size distribution of *B. subtilis* MutS variants at 10  $\mu$ M (dimer) and 220  $\mu$ M (tetramer) concentrations reveal similar oligomeric status.**

Samples were centrifuged at 15,700 x g for 10 minutes at 4°C and measured using a Zetasizer Nano S (Malvern Instruments) with a 4 mW He-Ne laser at 633 nm. All measurements were taken using a 12  $\mu$ L quartz cell (ZEN2112) at 4°C.

<i>Bacillus subtilis</i> MutS/ 306-330	EERQEMVETLM <b>SHFF</b> EREDLRERLK
<i>Homo sapiens</i> MSH3/ 14-38	SSSAPARQAVL <b>SRFF</b> QSTGSLKSTS
<i>Saccharomyces cerevisiae</i> MSH3/ 26-50	LLTIMAGQPTI <b>SRFF</b> KKAVKSELTH
<i>Homo sapiens</i> BLM/ 1308-1332	AEELDEEIPV <b>SHYF</b> ASKTRNERKR
<i>Homo sapiens</i> EXO1/ 493-517	ESGAVVVPGTR <b>SRFF</b> CSSDSTDCVS
<i>Saccharomyces cerevisiae</i> Ntg2/ 13-37	IPVDIEEVEVR <b>SKYF</b> KKNERTVELV
<i>Saccharomyces cerevisiae</i> Sgs1/ 1372-1396	SNGIAQSTG <b>TKSKFF</b> GANLNEAKEN
Consensus sequence	--S[HKR][YF]F--

**Figure S5. Overlay of the *B. subtilis* MutL binding site on MutS with the Mlh1 binding site on its binding partners.** Shown is an overlay of the *B. subtilis* MutL binding site on MutS with the MIP box (Mlh1 Interacting Protein box\_[R/K]-S-[H/R/K]-[Y/F]-F) reveals a conserved serine followed by the di-phenylalanine shared between the *B. subtilis* MutL binding site on MutS and Mlh1 binding partners in *S. cerevisiae*. The blue text in the overlay represents heavily conserved residues found within the MIP box, with the darkest blue representing the most conserved residues based on an eukaryotic Exo I alignment (Dherin *et al.*, 2009).

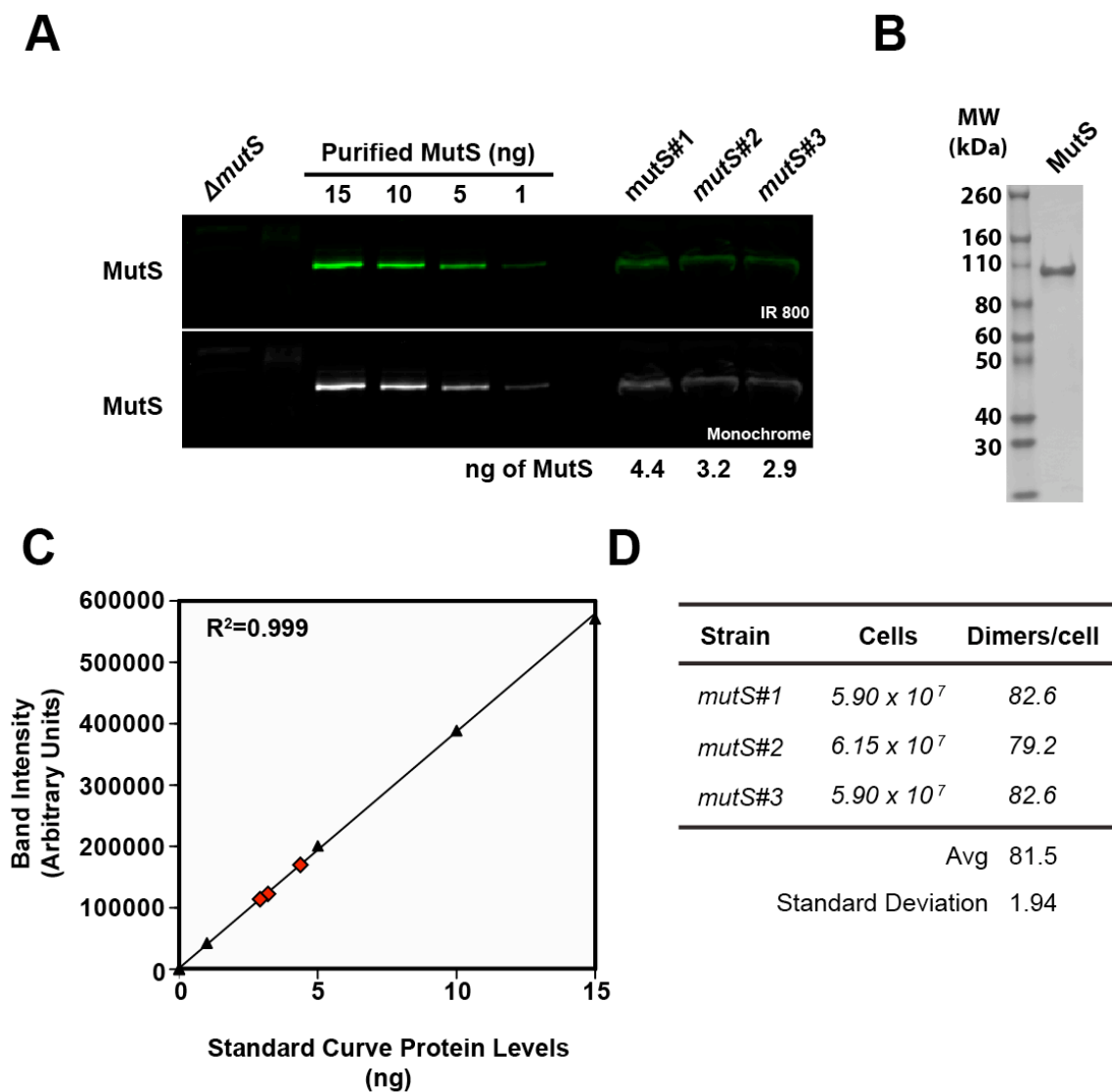


**Figure S6. Determination of the absolute number of MutS molecules in *B. subtilis*.**

**A)** The steady state levels of wild type MutS from whole cell extracts grown in the same conditions as those used for live cell microscopy were compared to a protein standard using purified MutS to determine the number of MutS molecules per cell. Band intensity was determined using LI-COR quantitative Western analysis technology. **B)** Image of 2  $\mu$ g of purified MutS used to construct the protein standard curve found in **A** on a 4-20% gradient gel. **C)**

Standard curve of purified MutS protein is pictured in **A**. Red squares indicate the coordinates of total MutS found within the extracts in **A**. **D**) A fraction of the culture used to make the whole cell extract was used to determine the number of viable cells by plating on LB agar. The cellular content of MutS within the whole cell extract was determined by adjusting the total ng of MutS identified in **A** and **C** by normalizing the amount of MutS to  $\text{g mol}^{-1}$  using the molecular weight of MutS (97394 Da), followed by multiplying by Avogadro's number ( $6.022 \times 10^{23}$ ) to obtain total molecules within the extract. This amount was divided by the total viable count of the culture to obtain the number of MutS monomers  $\text{cell}^{-1}$ . This number was further divided by 2 to obtain the number of dimers per cell. Determination of molarity (M) was based on *B. subtilis* cell lengths and widths under standard imaging conditions (avg. length=2.63  $\mu\text{m}$ , avg. width=0.83  $\mu\text{m}$ ,  $V_{\text{cyl}} \sim 5.32 \times 10^{-15}$  L, M=113 nM).

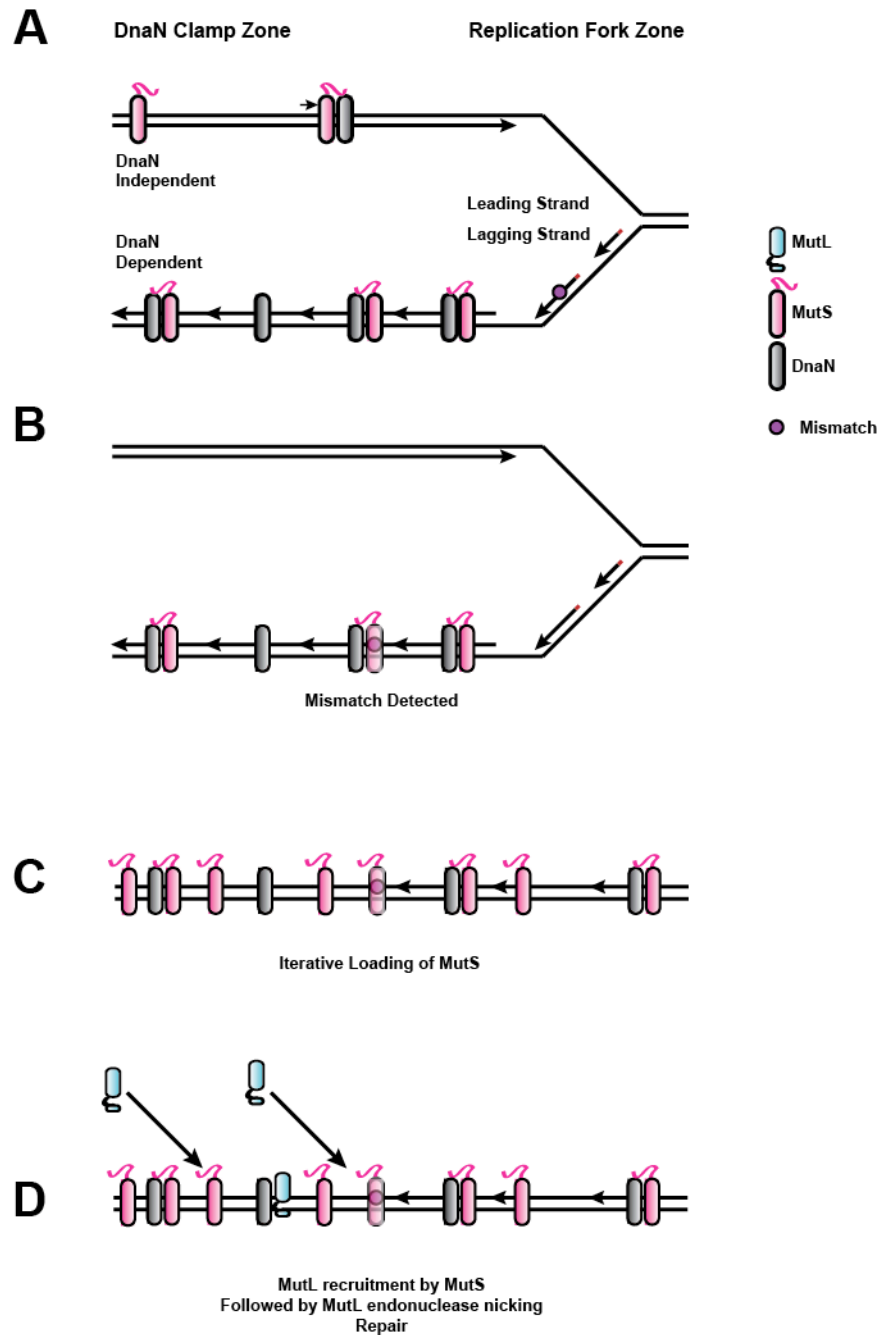


**Figure S7. A model of the initial steps of *B. subtilis* mismatch repair.** **A)** DnaN clamp zones direct MutS to newly replicated DNA to enhance mismatch detection. **B)** Mismatch detection by MutS. **C)** Iterative loading of MutS occurs at the site of the mismatch, which **D)** facilitates recruitment of MutL and endonuclease activation.

**Table S1. Individual amino acid substitutions that comprise each MutS patch variant.**

Patch designation	Residue substitutions	Domain
WT	None	
Patch 1	E155S, R156S, L157A, E158S	Connector
Patch 2	E245S, E247S, E248S	Connector
Patch 3a	E306S, E307S, E310S	Core
Patch 3b	F320S, E321S, R322S, E323S	Core
Patch 4	E392S, E395S, E396S	Core
Patch 5	E510S, E512S, E514S	Clamp
Patch 6a	Q806A, L807A, F809A, F810A	DnaN clamp binding
Patch 6b	D811S, E812S, E814S	DnaN clamp binding

Each amino acid substitution tested in the MutS patch mutants are listed and the domain location for each patch mutant is indicated based on the structural determination of bacterial MutS homologs (Lamers *et al.*, 2000, Obmolova *et al.*, 2000).

**Table S2: *B. subtilis* strains used in this study**

Strain	Relevant Genotype	Source or Reference
JSL364	PY79-Prototroph, SP $\beta$ <sup>o</sup>	(Youngman et al., 1984)
LAS393	<i>mutL::spec</i>	(Smith et al., 2001)
LAS435	<i>mutS::mutS-23-mgfpmut2-spec, mutL<sup>-</sup></i>	
JSL161	<i>mutL::mutL-23-mgfpmut2-spec</i>	
JSL305	$\Delta$ <i>mutSmutL-23-mgfpmut2-spec</i>	
JSL342	<i>mutS Patch 3B-1</i>	
JSL345	<i>mutS Patch 4-1</i>	
JSL346	<i>mutS Patch 5-6</i>	
JSL355	<i>mutS Patch 1-14</i>	
JSL372	<i>mutS Patch 3a</i>	
JSL377	<i>mutS Patch 2</i>	
JSL380	<i>mutSF320S (2-1)</i>	
JSL382	<i>mutS E321S</i>	
JSL386	<i>mutS Patch 6a-C2</i>	
JSL395	<i>mutS Patch 6b-3</i>	
JSL400	<i>mutS-22-mgfpmut3mutL<sup>+</sup></i>	

JSL402	<i>mutSF319SF320S</i>
JSL414	<i>mutSF320S-22-mgfpmut3mutL<sup>+</sup></i>
JSL416	<i>mutS R322S-1</i>
JSL419	<i>mutSE323S-1</i>
JSL424	<i>mutSF319S</i>
JSL425	<i>mutSF319SF320S-22-mgfpmut3mutL<sup>+</sup></i>
JSL438	<i>mutSF319SF320SmutL::mutL-23mgfpmut2-spec</i>
JSL440	<i>mutS-22mgfpmut3mutL::mutLE468K-cm</i>
JSL450	<i>mutSF319S-22mgfpmut3mutL<sup>+</sup></i>
JSL453	<i>mutSE323S-22mgfomut3mutL<sup>+</sup></i>
JSL455	<i>mutSF319SF320S-22mgfpmut3mutL<sup>+</sup>, dnaX::dnaX-23mCherry-spec</i>
JSL460	<i>mutS-22mgfpmut3mutL<sup>+</sup>, dnaX::dnaX-23mCherry-spec</i>
JSL467	<i>mutS Patch 3B-22mgfpmut3mutL<sup>+</sup></i>
JSL469	<i>mutSV206A, T207S, I208A, I209AmutL<sup>+</sup></i>
JSL471	<i>mutSS317A</i>
JSL473	<i>mutSH318S</i>

---

All strains listed are derivatives of PY79.

## References

- Dherin, C., E. Gueneau, M. Francin, M. Nunez, S. Miron, S. E. Liberti, L. J. Rasmussen, S. Zinn-Justin, B. Gilquin, J. B. Charbonnier & S. Boiteux, (2009) Characterization of a highly conserved binding site of Mlh1 required for exonuclease I-dependent mismatch repair. *Molecular and Cellular Biology* **29**: 907-918.
- Klocko, A. D., J. W. Schroeder, B. W. Walsh, J. S. Lenhart, M. L. Evans & L. A. Simmons, (2011) Mismatch repair causes the dynamic release of an essential DNA polymerase from the replication fork. *Mol Microbiol* **82**: 648-663.
- Lamers, M. H., A. Perrakis, J. H. Enzlin, H. H. Winterwerp, N. de Wind & T. K. Sixma, (2000) The crystal structure of DNA mismatch repair protein MutS binding to a G x T mismatch. *Nature* **407**: 711-717.
- Obmolova, G., C. Ban, P. Hsieh & W. Yang, (2000) Crystal structures of mismatch repair protein MutS and its complex with a substrate DNA. *Nature* **407**: 703-710.